The Earth planetary albedo surge in December 2020 validated using a weather prediction model

M. Vasiuta[1], L. Tuppi[1], A. Penttilä[2], K. Muinonen[2], and H. Järvinen[1]

[1]Institute for Atmospheric and Earth System Research, Faculty of Science, University of Helsinki, Finland
[2]Department of Physics, Faculty of Science, University of Helsinki, Finland

Key Points:

- The Deep Space Climate Observatory (DSCOVR) EPIC images indicate exceptionally large values of the Earth's planetary albedo in December 2020.
- Independent validation using a numerical weather prediction model suggests that this is an over-estimate.
- It may be partly attributed to a weakness of short-wave angular distribution models based on CERES/TRMM in full backscattering geometry.

Corresponding author: Maksym Vasiuta, `maksym.vasiuta@helsinki.fi`

Abstract

The focus here is on the Earth's planetary albedo estimates derived from the data of Earth Polychromatic Imaging Camera (EPIC) onboard NOAA's Deep Space Climate Observatory (DSCOVR). The estimates indicate a short-lived albedo surge with an instantaneous value of 0.350 on the 5th of December 2020 and a 5-day average above 0.330. A numerical weather prediction model-based (OpenIFS of ECMWF) estimate confirms the EPIC-based maximum in December 2020 but remains notably lower (maximum at 0.327). The discrepancy may be explained by the Earth–Satellite–Sun geometry since the DSCOVR satellite was very near the Lagrange point L1 and received the Earth outgoing short-wave radiation close to backscattering. In this conditions, the angular distribution model based on Clouds and the Earth's Radiant Energy System (CERES) and the associated footprint identification are prone to uncertainties.

Plain Language Summary

Albedo of the Earth is a key metric of the planet's energy balance. Earth-orbiting satellites are frequently used to measure reflected solar radiation on a global scale. It varies seasonally with maxima at solstices and minima at equinoxes. Pace of year-to-year changes is slow. However, measurements from year 2020 disclose an exceptionally large albedo maximum during Southern Summer solstice in December compared to the previous years. Here, we try to validate the maximum with independent means. We estimate the albedo using a global weather prediction model (OpenIFS) which indicates the albedo in year 2020 was likely at a fairly normal level. The question is: why does the EPIC camera on board NOAA's DSCOVR satellite measure so high albedo values. The answer seems to be in the fact that albedo retrieval from EPIC is sensitive to the Earth–Satellite–Sun geometry and footprints in satellite's field-of-view. In December 2020, the geometry was almost ideal backscatter situation with highly reflective Antarctic ice sheet fully exposed. The over-estimation may be attributed, at least in part, to these specific measurement conditions.

1 Introduction

The proportion of the incoming solar radiation reflected back to space by the Earth system is commonly known as the planetary albedo, a.k.a. spherical or Bond albedo. Various sources report (e.g., Stephens et al., 2015; Liang et al., 2019) that Earth planetary shortwave albedo is usually in the range of 0.3 ± 0.015. The annual maximum occurs in December around the Southern summer solstice, when the highly reflective Antarctic ice sheet and the cloudy Southern Ocean are fully exposed to sunlight. Interannual variablity of the planetary albedo is weak, not exceeding 0.5% of the annual mean value (Kato, 2009). Albedo estimates are mainly based on measurements of reflected shortwave radiation from Earth-orbiting satellites, which are translated to albedo values using reflectance modelling. In particular, the Clouds and the Earth's Radiant Energy System program (CERES) provides highly accurate instruments and algorithms to derive planetary albedo estimates (Wielicki et al., 2005).

Measurements from the Earth Polychromatic Imaging Camera (EPIC) onboard NOAA's Deep Space Climate Observatory (DSCOVR) are of particular interest for Earth's albedo studies. Since DSCOVR is located near the Earth Lagrange point L1, its field-of-view always contains almost the entire sunlit hemisphere of the Earth and thus within one snapshot provides necessary data for retrieving planetary albedo. The focus here is on a 5-year time-series of planetary albedo derived from the EPIC images (Penttilä et al., 2022). In their retrieval, the daily average of planetary albedo is 0.295 ± 0.024 except during December 2020 when this range is exceeded. In a consecutive period of three weeks, the albedo remains above 0.320 and one whole week in excess of 0.330. December 2020 is thus quite exceptional in this 5-year time-series. The immediate question is whether

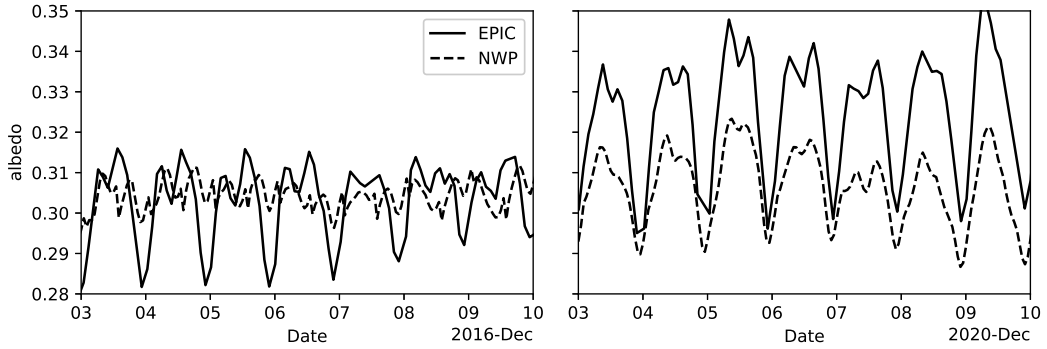

Figure 1. The planetary albedo of the Earth in 3–10 of December 2016 (left) and 3-10 of December 2020 (right) as derived from the OpenIFS model (dashed line) and the retrieval presented by Penttilä et al. (2022) (solid line).

the Earth system state — land and ocean surface and the atmosphere — was somehow exceptional, or can this anomaly be explained by some sensitivity in the retrieval method.

Reflective properties of the Earth's surface, the atmosphere, and clouds are highly varying and closely linked to the weather and climate. This explains why radiation quantities are key components in numerical weather prediction models, such as OpenIFS of the European Centre for Medium-Range Weather Forecasts. It is straightforward to use the OpenIFS radiation output at the top-of-atmosphere (ToA) to compute the Earth's planetary shortwave albedo based on its definition: total outgoing flux divided by total incoming flux, or

$$a_m = \frac{\sum_i N_i^{SW} A_i}{\sum_i N_i^{\odot} A_i}, \tag{1}$$

where a_m is the weather model-based short-wave planetary albedo, i denotes the weather model grid index, N_i^{SW} the ToA short-wave radiosity, $N_i^{\odot}$ the solar irradiance, and A_i the grid point surface area. For convenience, we denote by a_D the DSCOVR/EPIC measurements-based retrieval by Penttilä et al. (2022).

Figure 1 displays a_D (solid line) and a_m (dashed line) for December 2016 (left panel) and December 2020 (right panel) on a daily scale. According to Fig. 1, albedo estimate from OpenIFS shows smaller amplitude of daily variations and smaller daily maxima than the satellite-based retrieval both in 2016 and 2020. The daily mean values for a_m during 3-10 of December are 0.304 in 2016 and 0.307 in 2020, and 0.303 and 0.326 for a_D, respectively. According to OpenIFS, December 2016 and 2020 are fairly similar in terms of the Earth's planetary albedo. Curiously, the daily albedo variations are markedly higher in December 2020 than in 2016 in both data sets. Also, increase in albedo apparent in a_D is also present in a_m but it is far less pronounced. It is good to remember that the OpenIFS-based estimate is independent of the DSCOVR/EPIC measurement geometry (and, in general, of geometries of any other satellites) which is determined by the satellite orbit. The research question is thus: what are the factors lending to the apparent discrepancy in December 2020 between the two planetary albedo estimates?

2 Computation of albedo

Planetary albedo at any given moment is determined by the total reflected radiation exiting the Earth system in all directions. It is practically impossible to explicitly measure the total reflected radiation flux, and this fundamental limitation must be somehow overcome in measurement-based albedo retrieval (to obtain a_D). In numerical weather

prediction (NWP) models, the 3-dimensional radiative transfer is simplified into 1-dimensional where up/down fluxes are considered in each model grid column with no information about the angular distribution. The radiative transfer code is then calibrated with a range of Earth observations such that, e.g., heating rates due to radiation flux convergence are consistent. Obtaining a_m is thus straightforward while NWP model maintains consistency of radiation quantities.

2.1 Planetary albedo using L1-satellite-based imaging

The DSCOVR spacecraft orbits around the Lagrange point L1 in a Lissajous orbit (Koon et al., 2000) around 1.5 million kilometers from the Earth (Burt & Smith, 2012). This geometry allows viewing almost the entire sunlit hemisphere of the Earth. Its location is thus nearly-optimal for measuring the planetary albedo.

For planetary albedo retrieval, Penttilä et al. (2022) used data from the Earth Polychromatic Imaging Camera (EPIC) on board DSCOVR. These are time series of snapshot high-resolution images of the Earth's disk. The time series is irregular, having usually 22 images per day. Each image has 10 narrow-band channels spanning between 317 and 780 nm. An individual pixel represents directional radiance from the corresponding footprint of the Earth. The measured radiance is a function of reflective properties of a footprint, and the Sun–Earth–satellite geometry. In order to infer the total top-of-atmosphere (ToA) reflected radiosity based on these data (and thus, the global albedo), several processing steps are needed, as explained below.

First, a narrowband-to-broadband transformation is performed using pre-defined solar spectra convoluted with the EPIC transmittance of different channels. Despite the solar input within the EPIC channel range (from 317 to 780 nm) being only 52.7% of the total shortwave intensity, this range is sufficient to perform a narrowband-to-broadband transformation as described in Su et al. (2018). The directional broadband radiance is then converted to the total ToA radiosity for each pixel using angular distribution models (ADMs) of the CERES/TRMM project (Loeb et al., 2003). Each ADM comprises short-wave anisotropy factors in directions defined by the solar-zenith angle (SZA), observer-zenith angle (OZA), and azimuth angle of an observer relative to the solar plane (RA). The CERES/TRMM ADMs are tabulated for the following angles: $0° < \mathrm{SZA}, \mathrm{OZA} < 90°$ with $10°$ resolution, and $0° < \mathrm{RA} < 180°$ with $20°$ resolution.

The CERES/TRMM ADMs are parametrized based on the footprint reflective properties. There are thus different distribution functions for different footprint types. The main categories are clear ocean, clear land, and cloud-covered footprints. These ADMs are averages over all sub-categories, such as vegetation type and fraction, snow/ice cover, and cloud fraction.

Penttilä et al. (2022) modify the ADM table functions to benefit of the scattering geometry in the EPIC observations. First, the ADM tabulation are simplified to just one angular parameter — the solar-zenith angle. The specific location of DSCOVR satellite implies that the observing conditions are close to backscattering. Therefore, the relative azimuth (RA) angle is fixed, and the solar- and observer-zenith angles are almost equal. Second, the ADM tables are interpolated over the $0°$ to $90°$ range using a cubic spline interpolation. CERES/TRMM defines $\mathrm{RA} = 0°$ for forward-scattering, and $\mathrm{RA} = 180°$ for backscattering.

Lastly, Penttilä et al. (2022) modelled the effect of the phase angle (i.e., the satellite - the Earth - the Sun angle) on the global albedo estimation. The Earth's reflectance increases substantially when phase angle approaches zero, i.e., in full backscattering conditions (Marshak et al., 2021). The phase angle reached minimum of $1.8°$ in December 2020, while being in the range $5-11°$ in the year 2016. This phase angle condition explains about +0.010 increase of the albedo maximum in December 2020.

2.2 Planetary albedo using OpenIFS NWP model

OpenIFS is the atmospheric component of the Integrated Forecasting System (ECMWF, 2019, IFS, cycle 43r3) of the European Centre for Medium-Range Weather Forecasts (ECMWF). It is a portable weather model intended for academic use having identical forecast skill compared to the full IFS.

Our study uses the ECMWF initial states for December 2016 and December 2020, at 00 and 12 UTC. The planetary albedo estimates are produced as follows. We launch 16-hour forecasts from initial states with hourly output using the OpenIFS model. Hourly fields of the ToA outgoing and incoming shortwave radiation are extracted from the model output, and the albedo is computed using equation 1.

Evolution of the atmospheric state is simulated with OpenIFS resolution of $\mathrm{T_L}1279$ corresponding to about 18 km horizontal resolution at the equator, and at 137 vertical levels. The model top is at 0.01 hPa corresponding to about 80 km geometric altitude. Thus, the model domain covers the entire neutral atmosphere of the Earth. The model timestep is 10 minutes and the atmospheric state is output once an hour. To avoid the initial spin-up/down of the model hydrological cycle, the first forecast hour is discarded and forecast hours 2...13 are used instead.

The radiative transfer (the ecRad scheme Hogan & Bozzo, 2016) is solved in grid columns for solar and terrestrial components. Here, "solar" refers to radiation scattered, reflected, or transmitted by the Earth system at $0.2 - 4$ µm wavelength interval, and "terrestrial" to radiation emitted by the surface or by the atmosphere at the interval of $4 - 100$ µm. These two intervals have some overlap since the division means separating its origin, rather than separating energy flux with a 4 µm wavelength threshold. The radiative transfer computation in OpenIFS is performed once an hour in this study.

The ecRad scheme is quite precise having ToA radiosity uncertainty of about 0.1 $\mathrm{Wm^{-2}}$ (Hogan & Bozzo, 2016, Table 2). Yet, the local albedo estimate, which depends on the local atmospheric state, is uncertain since the model state differs from the true state. However, the global albedo uncertainty is driven mostly by the global net radiation imbalance in the model, which is at the level of 1 $\mathrm{Wm^{-2}}$ (≈ 0.003 albedo units; Roberts et al. (2018)).

3 Validation hypothesis and methods

There is a significant difference between the two independent albedo estimates, as shown on Figure 1. In December 2020, the global ToA short-wave radiosity is on average 6.5 $\mathrm{Wm^{-2}}$ larger in EPIC estimate than in the OpenIFS model. Thus, the conversion of the EPIC radiance to ToA radiosity appears to be overestimated. Hence, the corresponding reverse radiosity-to-radiance conversion would be underestimated. We developed an improved radiosity-to-irradiance conversion by applying the CERES ADMs with a broader parametrization scheme. We expect, the new conversion would not be underestimated contrary to the conversion by Penttilä et al. (2022).

Within the concept of different conversions from radiosity to irradiance, validation of the planetary albedo narrows to a task of comparing amounts of irradiance received by the satellite from the visible Earth disk. In the new conversion, we applied the CERES ADMs to OpenIFS ToA radiosity considering the orbit geometry of DSCOVR satellite. The validation hypothesis is as follows. The Earth irradiance of the DSCOVR satellite based on OpenIFS should agree with the Earth irradiance measured by the satellite.

The short-wave irradiance of the DSCOVR satellite from a single OpenIFS grid cell is

$$E = \frac{N}{\pi} R_x(\theta_0, \theta, \phi) \frac{A \cos\theta}{r^2}\,, \tag{2}$$

where E is the scalar irradiance (Wm^{-2}), N the ToA radiosity from a single grid cell (Wm^{-2}), $R_x(\theta_0, \theta, \phi)$ the angular distribution function for footprint type x of solar-zenith θ_0, satellite-zenith θ, and relative azimuth ϕ angles, A the surface area of a footprint (m^2), and r the footprint-satellite distance (m). Tabulated CERES angular distribution functions are interpolated over their defined range using tri-linear interpolation.

DSCOVR satellite has NIST Advanced Radiometer (NISTAR) on board. It observes reflected and emitted radiation of the Earth's sunlit hemisphere with single pixel active cavity radiometer measurements in full spectrum (Band-A, $0.2 - 100$ µm), and in filtered broad bands (Band-B, $0.2-4$ µm, and Band-C, $0.7-4$ µm). Band-B data coincide with the spectral domain of short-wave radiation of the OpenIFS model. The raw irradiance measurements are made every 10 seconds, however, we use hourly values from a moving average with 4-hour window (Level 1B).

3.1 Connecting Angular Distribution Models with OpenIFS model variables

The CERES/TRMM ADMs are stratified by scene types defined by parameters that have a strong influence on the angular dependence of the Earth's outgoing radiation at ToA. The parameter space corresponds to almost 600 unique footprint types. The OpenIFS model provides output variables and parameters that can be connected with the CERES ADMs, as explained next.

Clear-sky ocean ADMs are parametrized by surface wind speed, and the corresponding OpenIFS variable is the 10 metre wind speed (unit: m/s). The cloudy-ocean footprint is parametrized by cloud cover fraction, micro-physical phase, and optical depth. Here, the OpenIFS variables are cloud cover (cloud fraction) and column liquid water and ice (unit: kg m^{-2}). Optical depth τ is calculated according to Petty (2006):

$$\tau = \frac{3L}{2\rho r_{\mathrm{eff}}}\,, \tag{3}$$

where L is the liquid/ice water content, ρ the water/ice density (g cm^{-3}), and r_{eff} the effective droplet/crystal size (µm). Effective particle size r_{eff} is not provided in the model output. It is fixed to 15 µm here. Micro-physical phase at the cloud top is not resolved, hence we use the average over liquid and ice ADMs.

Clear-sky land is parametrized by four types of vegetation foliage derived from land cover classification scheme IGBP (Friedl et al., 2010). OpenIFS operates Hydrology Tiled ECMWF Scheme for Surface Exchanges over Land (HTESSEL) (Balsamo et al., 2009), which differs from IGBP. We mapped HTESSEL scheme onto land cover types defined by CERES/TRMM. Clouds-over-land ADMs have the same land cover parameters as the clear-sky land, and added with cloud cover fraction, micro-physical phase, and optical depth.

CERES/TRMM does not provide parametrization over snow and ice cover, because the Earth view by the mission was limited to $\pm 38^\circ$ of latitude. We used snow and ice ADMs from CERES/Terra, supplementing them with climatological permanent snow cover (in m of water equivalent).

4 Results

The hypothesis is tested next. We produced time series of the simulated short-wave DSCOVR irradiance for December 2020. We compared the result with the NISTAR Level 1B hourly data. In Figure 2 (top), shortwave irradiance by OpenIFS+CERES (dashed line) is systematically lower than the NISTAR Band-B unfiltered measurements (solid line), on average by more than 10%. Daily and amplitude variations, and tendencies are

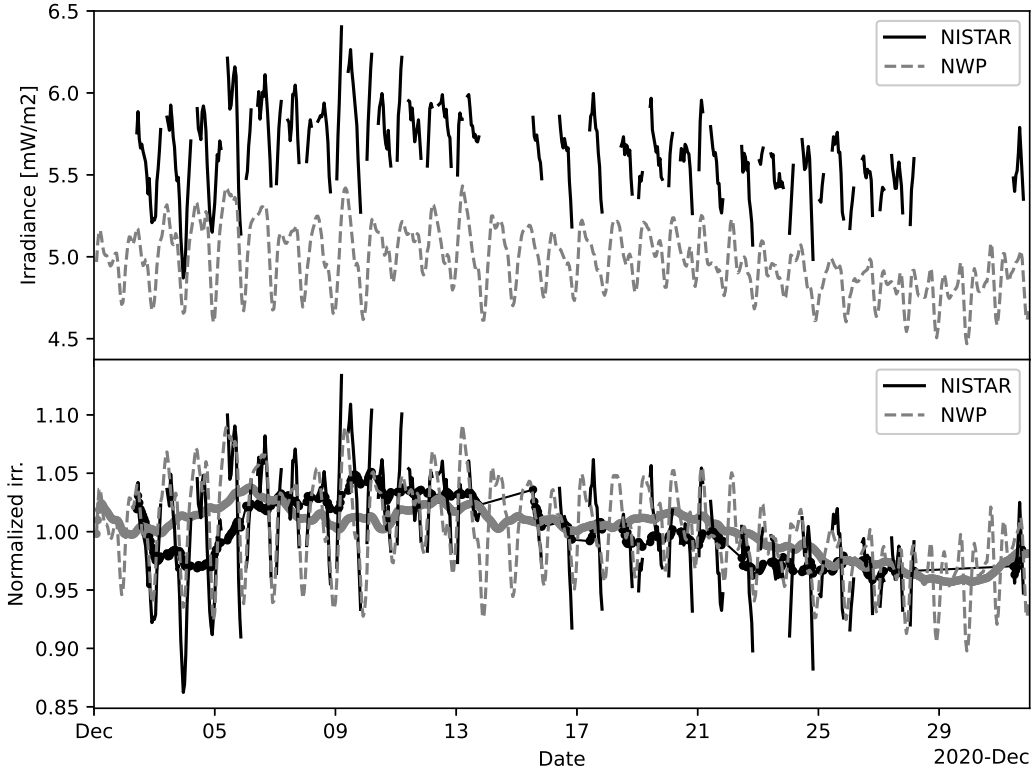

Figure 2. The measured (black solid line) and simulated (gray dashed line) shortwave Earth irradiance received by DSCOVR satellite during December 2020, with hourly frequency. The top figure shows original time series, on the bottom - time series are divided by their mean and smoothed with 24-hour moving average. Mean observed irradiance: 5.648 mW/m^2, mean simulated irradiance: 4.986 mW/m^2 Computations are done by integrating directional radiance over the visible Earth disc, as described by equation 2.

generally well-captured by the simulation. Unfortunately, NISTAR measurements are not available for December 2016.

Figure 3 illustrates the short-wave radiation anisotropy factors (i.e., values of the interpolated angular distribution functions) of CERES/TRMM and CERES/Terra ADMs together with a human-eye view of the Earth by EPIC imagery. Here, we visually demonstrate the classification of footprints using the OpenIFS model output connected with the CERES ADM parameters. Artifacts due to 10° resolution of the ADMs are visible as concentric rings within the disk. Curiously, glint and effect of non-zero phase angle (equals 2.1° at that time) are seen near the Earth's sub-solar point.

In addition, we estimated so-called 'opposition effect' of the visible Earth disk. Figure 4 shows the surge in disk-integrated brightness along with DSCOVR phase angle values during December 2020. The simulated effect is computed by integrating the ADM anisotropy factors over the disk, and the "observed" effect is time-interpolated NISTAR Band B irradiance divided by the irradiance from the OpenIFS model Earth assuming the Earth being an ideal Lambertian scatterer ($R_x(\theta_0, \theta, \phi) \equiv 1$). The "observed" value is larger than the simulated (range from 1.16 to 1.43 against $1.12 - 1.20$). According to Fig. 4, the complex daily variability of the "observed" effect is weakly captured in the simulated effect time series. Notably, the value of 'opposition effect' is strongly associ-

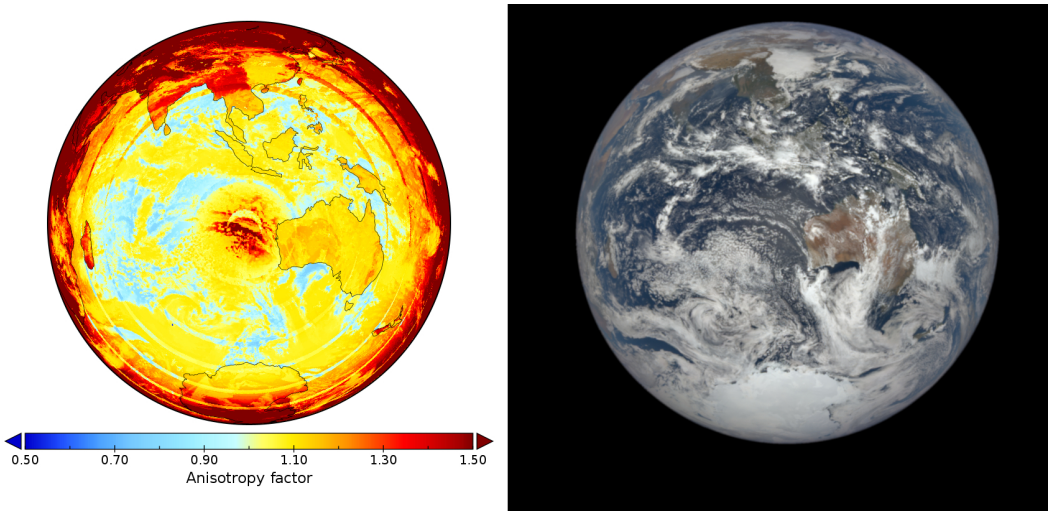

Figure 3. EPIC 1b natural colour image taken at 2020-12-13 04:40:41 UTC (right) and corresponding anisotropy factors R_x from CERES/TRMM and CERES/Terra ADMs using the OpenIFS fields for scene classification (left). Date and time of the simulation: 2020-12-13 05:00 UTC.

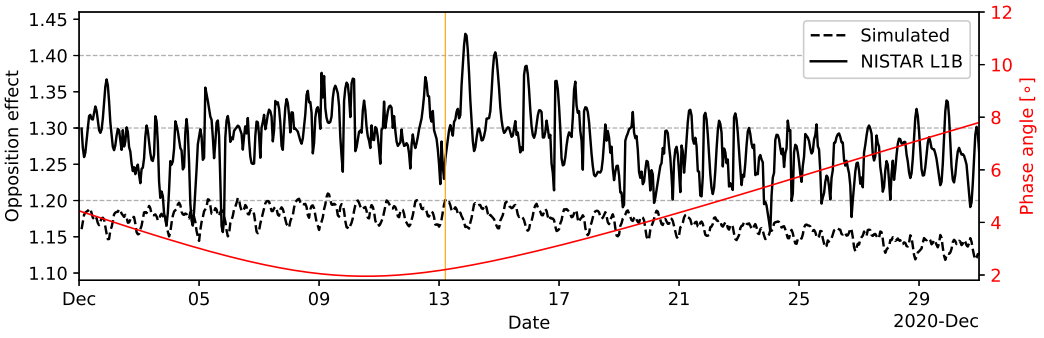

Figure 4. Observed (solid black line) and simulated (dashed black line) disk-integrated anisotropy factors ('opposition effect') and DSCOVR phase angle time series (red line) for December 2020. The epoch of Figure 3 is marked with the orange line.

ated with the phase angle, supporting findings of Marshak et al. (2021). Pearson correlation coefficient is -0.43 for the "observed", and -0.83 for the simulated effect.

5 Discussion

The validation hypothesis is based on comparison of the simulated and the observed irradiance of DSCOVR satellite on an hourly scale. DSCOVR unique location in a Lissajous orbit around L1 point implies near-backscattering viewing geometry of the Earth. In this situation however, irradiance-to-radiosity conversion needed to estimate the planetary albedo is highly sensitive to weather and land cover properties, and to rapidly changing viewing geometry due to rotation of the Earth.

The validation hypothesis is rejected by NISTAR data in December 2020, and two possible reasons may contribute to the rejection. First, the Earth footprints classification scheme in CERES ADMs may not be fully applicable to the OpenIFS model data.

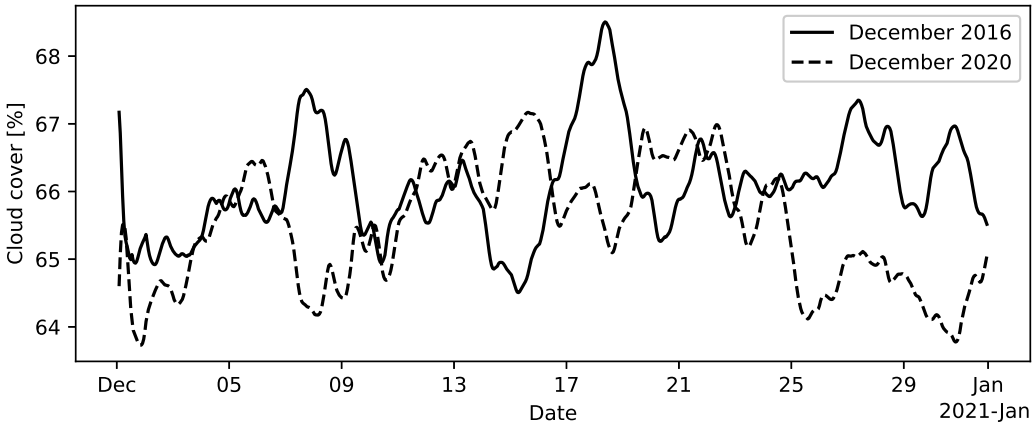

Figure 5. Total cloud cover over water bodies in view of DSCOVR satellite produced from the OpenIFS output in December 2016 (solid) and December 2020 (dashed). The cloud cover time series are shown as 24-hour window moving averages.

Second, the ADMs have substantial errors when close to backscattering, underestimating the anisotropic factors of the Earth outgoing short-wave radiation. We hope the newest ADMs (Su et al., 2015, for example) are able to mitigate these potential weaknesses. However, this model is not yet available as a standalone product.

The insight into these two aspects is the following. It is hard to quantify the quality of the classification scheme and its correspondence to numerical weather data. Yet, weather phenomena and land cover features are captured, and ought to deal noticeable impact on short-wave directional brightness of the Earth, as demonstrated in Figure 3. Also, underestimation of the anisotropic factors is substantial, as demonstrated in Figure 4.

In addition, we estimated one of the proxies for planetary albedo: the cloud coverage. We assessed the ocean cloud fraction that is in the field of view of DSCOVR satellite (i.e., on sunlit hemisphere). Abundant cloud cover is an indicator of a larger-than-usual planetary albedo, suggesting the proxy was larger during December 2020 compared to December 2016. Despite the suggestion, there is no increase in cloud coverage over the sunlit ocean in December 2020 with respect to December 2016, as seen from the OpenIFS data shown at Figure 5.

6 Conclusions

The short-lived increase in global albedo by more than 0.020 in December 2020 is not confirmed with approach based on OpenIFS model. The reason of such a high albedo retrieved from the EPIC measurements is that the phase angle of DSCOVR satellite decreased to 1.8° at that time. CERES/TRMM angular distribution models, used to reconstruct the Earth short-wave top-of-atmosphere radiosity, seem to underestimate the Earth reflectance for this near-backscattering geometry.

Validation of the Earth's planetary albedo is based on the forward-modelling of broadband irradiance of a satellite: approach is reversed to estimating broadband planetary albedo from the satellite measurements. The input of such forward-modelling is the NWP model output supplied with parameterised empiric ADMs. We adopted the classification of the Earth's footprints according to their reflective properties by using detailed

weather and climate products from OpenIFS and ECMWF. We hereby are able to connect the weather model variables as an input to empiric angular distribution functions, and diagnose them.

Open Research Section

The Earth's planetary shortwave albedo retrievals are available at `https://albedo.physics.helsinki.fi`. The raw data by DSCOVR is available at the NASA EarthData site at `https://asdc.larc.nasa.gov/data/DSCOVR`. Availability of the OpenIFS initial states is described in Ollinaho et al. (2021). OpenIFS model requires a license for usage. See `https://confluence.ecmwf.int/display/OIFS/OpenIFS+Licensing` for details. Radiation angular distribution models are provided by CERES, and available at CERES (2015).

Acknowledgments

Funding

We gratefully acknowledge support of the Doctoral Programme in Atmospheric Sciences in the University of Helsinki, and funding received from the Academy of Finland (grant No. 1333034), the Vilho, Yrjö and Kalle Väisälä Foundation and Magnus Ehrnrooth Foundation. Research by KM and AP supported by the Academy of Finland (Research Council of Finland grants No. 1345115 and 1336546). We would like to thank CSC — IT Center for Science Ltd. in Finland – for their provision of computational resources.

Author contributions

Conceptualization: KM, AP, HJ

Data curation: MV, LT

Formal Analysis: MV

Funding acquisition: HJ

Investigation: HJ, MV

Methodology: MV

Project administration: HJ, MV

Resources: LT

Software: MV, AP

Supervision: HJ

Validation: MV

Visualization: MV

Writing – original draft: MV, LT, HJ

Writing – review & editing: MV, LT, HJ, AP, KM

Competing interests

Authors declare that they have no competing interests.

References

Balsamo, G., Beljaars, A., Scipal, K., Viterbo, P., van den Hurk, B., Hirschi, M., & Betts, A. K. (2009). A revised hydrology for the ecmwf model: Verification from field site to terrestrial water storage and impact in the integrated forecast system. *Journal of hydrometeorology*, *10*(3), 623–643.

Burt, J., & Smith, B. (2012). Deep space climate observatory: The dscovr mission. In *2012 ieee aerospace conference* (pp. 1–13).

CERES. (2015). *Angular distribution models* [dataset]. Retrieved from `https://ceres.larc.nasa.gov/data/angular-distribution-models`

ECMWF. (2019). *Changes in ecmwf model* [software]. Retrieved from `https://www.ecmwf.int/en/forecasts/documentation-and-support/changes-ecmwf-model`

Friedl, M., Strahler, A., Hodges, J., Hall, F., Collatz, G., Meeson, B., ... Landis, D. (2010). Islscp ii modis (collection 4) igbp land cover, 2000-2001. *ORNL DAAC*.

Hogan, R. J., & Bozzo, A. (2016). *Ecrad: A new radiation scheme for the ifs*. European Centre for Medium-Range Weather Forecasts.

Kato, S. (2009, SEP 21). Interannual variability of the global radiation budget. *Journal of climate*, *22*(18), 4893-4907. doi: 10.1175/2009JCLI2795.1

Koon, W. S., Lo, M. W., Marsden, J. E., & Ross, S. D. (2000). Dynamical systems, the three-body problem and space mission design. In *Equadiff 99: (in 2 volumes)* (pp. 1167–1181). World Scientific.

Liang, S., Wang, D., He, T., & Yu, Y. (2019). Remote sensing of earth's energy budget: synthesis and review. *International Journal of Digital Earth*, *12*(7), 737-780. Retrieved from `https://doi.org/10.1080/17538947.2019.1597189` doi: 10.1080/17538947.2019.1597189

Loeb, N. G., Manalo-Smith, N., Kato, S., Miller, W. F., Gupta, S. K., Minnis, P., & Wielicki, B. A. (2003). Angular distribution models for top-of-atmosphere radiative flux estimation from the clouds and the earth's radiant energy system instrument on the tropical rainfall measuring mission satellite. part i: Methodology. *Journal of applied meteorology*, *42*(2), 240–265.

Marshak, A., Delgado-Bonal, A., & Knyazikhin, Y. (2021). Phase angle and the estimation of earth reflectance. In *Agu fall meeting abstracts* (Vol. 2021, pp. A25F–1727).

Ollinaho, P., Carver, G. D., Lang, S. T. K., Tuppi, L., Ekblom, M., & Järvinen, H. (2021). Ensemble prediction using a new dataset of ecmwf initial states – openensemble 1.0. *Geoscientific Model Development*, *14*(4), 2143–2160. Retrieved from `https://gmd.copernicus.org/articles/14/2143/2021/` doi: 10.5194/gmd-14-2143-2021

Penttilä, A., Muinonen, K., Ihalainen, O., Uvarova, E., Vuori, M., Xu, G., ... Marshak, A. (2022). Temporal variation of the shortwave spherical albedo of the earth. *Frontiers in Remote Sensing*, *3*. Retrieved from `https://www.frontiersin.org/articles/10.3389/frsen.2022.790723` doi: 10.3389/frsen.2022.790723

Petty, G. W. (2006). *A first course in atmospheric radiation*. Sundog Pub.

Roberts, C. D., Senan, R., Molteni, F., Boussetta, S., Mayer, M., & Keeley, S. P. (2018). Climate model configurations of the ecmwf integrated forecasting system (ecmwf-ifs cycle 43r1) for highresmip. *Geoscientific model development*, *11*(9), 3681–3712.

Stephens, G. L., O'Brien, D., Webster, P. J., Pilewski, P., Kato, S., & Li, J.-l. (2015). The albedo of earth. *Reviews of Geophysics*, *53*(1), 141-163. Retrieved from `https://agupubs.onlinelibrary.wiley.com/doi/abs/10.1002/2014RG000449` doi: 10.1002/2014RG000449

Su, W., Corbett, J., Eitzen, Z., & Liang, L. (2015). Next-generation angular distribution models for top-of-atmosphere radiative flux calculation from ceres

instruments: methodology. *Atmospheric Measurement Techniques*, *8*(2), 611–632. Retrieved from https://amt.copernicus.org/articles/8/611/2015/ doi: 10.5194/amt-8-611-2015

Su, W., Liang, L., Doelling, D. R., Minnis, P., Duda, D. P., Khlopenkov, K., ... Rose, F. G. (2018). Determining the shortwave radiative flux from earth polychromatic imaging camera. *Journal of Geophysical Research: Atmospheres*, *123*(20), 11,479-11,491. Retrieved from https://agupubs.onlinelibrary.wiley.com/doi/abs/10.1029/2018JD029390 doi: https://doi.org/10.1029/2018JD029390

Wielicki, B. A., Wong, T., Loeb, N., Minnis, P., Priestley, K., & Kandel, R. (2005). Changes in earth's albedo measured by satellite. *Science*, *308*(5723), 825–825. doi: 10.1126/science.1106484